RSC Advances

COMMUNICATION

View Article Online
View Journal | View Issue

$Na_2FeP_2O_7$ as a positive electrode material for rechargeable aqueous sodium-ion batteries†

Cite this: *RSC Adv.*, 2014, **4**, 9799

Young Hwa Jung, Chek Hai Lim, Joo-Hyung Kim and Do Kyung Kim*

Received 12th December 2013
Accepted 28th January 2014

DOI: 10.1039/c3ra47560c

www.rsc.org/advances

An iron-based pyrophosphate compound, $Na_2FeP_2O_7$, is investigated as a positive electrode material for aqueous sodium-ion batteries for the first time. The high rate capability and good cyclability of this material in aqueous electrolytes are advantageous for low-cost and safe battery systems.

The increase of energy consumption and the demand for environmental energy resources have generated numerous investigations concerning several types of rechargeable batteries. In particular, research on rechargeable sodium-ion batteries (SIBs) has been promoted to utilize large energy storage systems (ESSs) as an alternative to lithium-ion batteries (LIBs) due to considerations of price and abundance in the world.[1–3] While interest in SIBs has grown, concerns over safety using both Na metal as an anode and flammable organic solvents as electrolytes similar to the Li case have also arisen. Safety and a low price are the most important aspects of large-scale battery systems; hence, aqueous SIBs are attractive candidates to satisfy both these safety and cost requirements. In addition, aqueous solutions have further advantages of easy preparation, non-toxicity, and higher ionic conductivity than the currently employed organic solvents.

Despite these advantages of aqueous electrolytes, aqueous batteries have been troubled with the following drawbacks – a narrow potential window limited by the decomposition of water, the dissolution of electrode materials in aqueous solutions, and a short lifetime due to side reactions. Since Li *et al.* first introduced the feasibility of aqueous LIBs based on intercalation compounds,[4] various types of electrode materials have been scrutinized for aqueous rechargeable batteries.[5] Whereas most of the studies in aqueous systems have been focused on Li compounds, only a few sodium ion insertion materials in aqueous electrolytes have been studied compared with considerable investigations of sodium intercalative materials in nonaqueous electrolytes.[6–13] Considering the requirements in aqueous batteries, the electrode materials for sodium aqueous systems are still limited. Therefore, the search for electrode materials that are inexpensive, easy to synthesize, stable, safe, non-toxic, long-lasting, and fit in the suitable potential in aqueous systems is necessary for the development of safe and inexpensive aqueous SIBs.

Recently, various pyrophosphate compounds have attracted attention as Na electrode materials due to their stable structure, good capacity retention, and high thermal stability.[14–21] Among these compounds, sodium iron pyrophosphate ($Na_2FeP_2O_7$) exhibits a reversible capacity of ~80 mA h g^{-1} at approximately 3 V *vs.* Na^+/Na, an appropriate potential range for neutral aqueous electrolytes. In particular, iron-based compounds have an advantage in terms of price, which is a considerable factor for the application of SIBs. Moreover, its 3D framework provides facile ionic conduction through its open channels, which are able to accommodate several sodium sites. Inspired by the impressive electrochemical characteristics of $Na_2FeP_2O_7$ in organic electrolytes as well as the cost merit and robust crystal structure, we introduce here an iron-based sodium intercalative material, $Na_2FeP_2O_7$, as a positive electrode for aqueous SIBs for the first time.

$Na_2FeP_2O_7$ has been synthesized as a carbon composite form to overcome the intrinsic low electronic conductivity of the pyrophosphate compound. Fig. 1a presents the Rietveld refinement results with the synchrotron X-ray diffraction patterns of the as-synthesized $Na_2FeP_2O_7$/C composite. The crystal structure of the composite was refined as a triclinic unit cell ($P\bar{1}$, no. 2), starting from the structure of the recently reported $Na_2FeP_2O_7$.[21] The refined lattice parameters are a = 6.3899(2) Å, b = 9.4562(2) Å, c = 11.020(1) Å, α = 63.738(1)°, β = 84.729(2)°, γ = 73.113(2)° and V = 570.88(3) Å^3, respectively (R_{wp} = 7.28%, R_p = 5.63%, $R(F^2)$ = 5.48% and χ^2 = 1.95). This crystal structure is the same as that of $Na_{4-\alpha}M_{2+\alpha/2}(P_2O_7)_2$ (M = Fe, Mn, Ni),[17,22] which is different from that of the first published

Department of Materials Science and Engineering, Korea Advanced Institute of Science and Technology (KAIST), 291 Daehak-ro, Yuseong-gu, Daejeon, 305-701, Republic of Korea. E-mail: dkkim@kaist.ac.kr

† Electronic supplementary information (ESI) available. See DOI: 10.1039/c3ra47560c

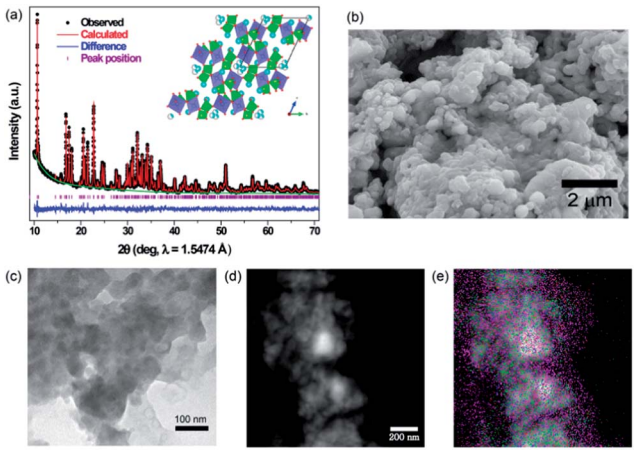

Fig. 1 (a) The synchrotron diffraction data with Rietveld refinement of $Na_2FeP_2O_7$/C. The inset shows the crystal structure of the refined $Na_2FeP_2O_7$ along the [1 0 0] direction. (b) An SEM image, (c) a TEM image and (d) an STEM image of the as-synthesized $Na_2FeP_2O_7$/C. (e) An EDS mapping for C (purple), Na (red), Fe (blue) and P (green).

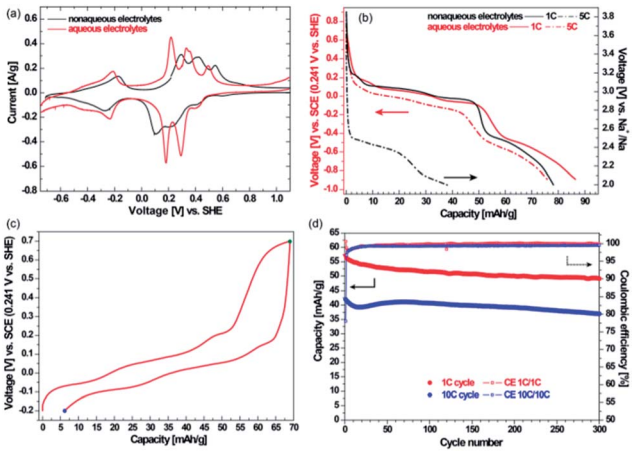

Fig. 2 (a) CV curves of the $Na_2FeP_2O_7$/C electrode in nonaqueous and aqueous electrolytes, (b) galvanostatic discharge curves of $Na_2FeP_2O_7$/C at a rate of 1 C and 5 C in nonaqueous and aqueous electrolytes, (c) galvanostatic voltage-capacity profile at the C/5 rate in aqueous electrolytes, and (d) capacity retention at 1 C and 10 C-rate in aqueous electrolytes.

$Na_2FeP_2O_7$.[14,16] However, the atomic ratio of Na, Fe and P was same to that of $Na_2FeP_2O_7$ from detailed refined parameters, as demonstrated in Table S1.† In parallel, the atomic ratio by ICP analysis was confirmed to be Na : Fe : P = 2 : 0.96 : 1.98. Therefore, we render this material as $Na_2FeP_2O_7$, as already published elsewhere. The inset of Fig. 1a shows the crystal structure of the refined $Na_2FeP_2O_7$ along the [1 0 0] direction. Sodium ions are accommodated at six sites; Na1, 2, and 3 with full occupancy and Na4, 5, and 6 with partial occupancy. The crystal structure consists of infinite arrays of $[P_2O_7]$ and $[FeO_6]$ octahedra, which provide a 3-dimensonal framework for sodium ions to migrate efficiently.

The morphology of the powders is depicted in Fig. 1b and c. The particles are agglomerated, and the diameter of the individual particles varies between 50 nm and 200 nm. The relatively small particle size may arise from the low synthetic temperature (600 °C) and from the carbon source (glycine) preventing particle growth. In addition, Fig. 1d and e also confirm the distribution of agglomerated powders based on the scanning transmission electron microscopy (STEM) and energy-dispersive spectroscopy (EDS) elemental mappings of the $Na_2FeP_2O_7$/C composite. It can be clearly observed that carbon is homogeneously distributed all over the range of the particles, and Na, Fe and P are also uniformly detected inside the bulk of the particles (Fig. S1†). Additionally, the carbon content of the composite is confirmed to approximately 15% using the element analyzer.

Fig. 2a presents two cyclic voltammograms of $Na_2FeP_2O_7$/C in nonaqueous and aqueous electrolytes. The potential was converted into voltage *vs.* SHE (standard hydrogen electrode). A similar set of four redox peaks is present in both CV curves during oxidation and reduction; however, it is apparent that the intensities and shapes of the CV peaks in the aqueous electrolytes are more sharp and clear, and the polarization of each redox peak in the aqueous electrolytes is also reduced compared with that in the organic solvents, indicating faster kinetics in the aqueous electrolytes. In the aqueous electrolytes, five anodic current peaks at −0.21, 0.21, 0.33, 0.36 and 0.49 V *vs.* SHE (corresponding to 2.50, 2.92, 3.04, 3.07 and 3.20 V *vs.* Na^+/Na) are observed during the oxidation process, which is consistent with previously reported results for $Na_2FeP_2O_7$ in nonaqueous electrolytes regardless of the crystal structures.[14,16] In addition, the single anodic peak at 0.42 V in the organic solvent electrolytes is slightly split into two peaks at 0.33 and 0.36 V in the aqueous solvents, in parallel to the data at the slower scan rate in the organic electrolytes,[14] which also suggests rapid ionic diffusion in aqueous electrolytes. During the reduction process, there are four corresponding cathodic current peaks at −0.23, 0.18, 0.29 and 0.41 V *vs.* SHE. Similarly, the galvanostatic discharge profiles at 1 C and 5 C in nonaqueous and aqueous electrolytes are displayed in Fig. 2b. The profiles at the low C-rate (1 C) exhibit a similar distinctive voltage plateau in the two electrolytes; however, at the higher rate (5 C), the IR drop of $Na_2FeP_2O_7$/C in the nonaqueous electrolytes is much larger than that in the aqueous electrolytes. Hence, the capacity at the high C-rate in the nonaqueous electrolyte is much lower (~40 mA h g^{-1}, half of the capacity at 5 C in the aqueous electrolytes) than that in the aqueous electrolytes. These trends are consistent with the previously reported results about electrode materials in organic solvents and aqueous solutions;[11,23] it is generally accepted that the higher rate capability in aqueous electrolytes is attributed to the high ionic diffusivity of aqueous electrolytes. Additionally, $Na_2FeP_2O_7$/C in aqueous systems exhibits excellent rate capabilities (Fig. S2†). 40% of the initial capacity was still retained even when the C-rate is increased 250-fold from 0.2 to 50 C.

The electrochemical Na insertion/extraction process is believed to be consistent for both electrolytes in the same potential range based on the CV data and galvanostatic voltage profiles. Even though $Na_2FeP_2O_7$/C shows the high reversibility and rate capability in aqueous electrolytes, one concern appears

over the active voltage region that can be applied to the practical area because the reaction potential of the material covers the full range from −0.654 V to 0.576 V *vs.* SCE (Standard Calomel Electrode) in neutral aqueous solution. Thus, a suitable voltage region for a positive or a negative electrode for aqueous SIBs should be selected; the usable potential range from −0.2 V to 0.7 V *vs.* SCE (corresponding to 0.041 V to 0.941 V *vs.* SHE) is selected to further electrochemically test for $Na_2FeP_2O_7$. This range suggests that two-thirds of full capacity can be utilized, similar to the case of $Na_{0.44}MnO_2$ as a positive electrode material for aqueous SIBs.[6,23] Fig. 2c illustrates the galvanostatic voltage-capacity curve of the $Na_2FeP_2O_7$/C electrode between −0.2 V and 0.7 V *vs.* SCE at a rate of 0.2 C (19.4 mA g^{-1}). Despite the relatively low coulombic efficiency (~93%) at 0.2 C, the battery delivers approximately 65 mA h g^{-1} of discharge capacity in a narrow voltage region. The initial coulombic efficiency increased at the 1 C and 10 C-rate in the same voltage range, and the value could be enhanced over 99.5% after 30 cycles, as illustrated in Fig. 2d. It is evident that $Na_2FeP_2O_7$ in aqueous electrolytes exhibits decent capacity retention in spite of the narrow voltage range. The initial discharge capacity is 58 mA h g^{-1} between −0.2 and 0.7 V *vs.* SCE, and the capacity retention is approximately 86% after 300 cycles at the 1 C-rate. Even at the high rate of 10 C, the cell exhibits a comparable lifetime; the capacity retains approximately 37 mA h g^{-1} after 300 cycles of charge and discharge at the 10 C-rate. The detailed voltage-capacity profiles of the 1 C and 10 C cycles are displayed in Fig. S3.† To compare the cyclability in nonaqueous electrolytes with the same voltage range, the cycling data and voltage profiles at 1 C cycles in nonaqueous electrolytes are presented in Fig. S4.† Although $Na_2FeP_2O_7$ is reported to have stable cyclability in nonaqueous electrolytes,[14,17] the capacity retention in the narrow voltage region is gradually decreased due to the enforced voltage cut-off over the potential plateau at approximately 3 V *vs.* Na^+/Na. Moreover, only half of the capacity (25 mA h g^{-1}) could be produced in organic electrolytes at 1 C in the limited voltage range, further supporting the higher kinetics and stability of $Na_2FeP_2O_7$ in aqueous electrolytes.

It can be inferred that the reversible electrochemical reaction of $Na_2FeP_2O_7$/C in aqueous electrolytes does not originate from the side reaction of aqueous electrolytes but instead from the phase transition by the redox couple of Fe based on the analogous CV and galvanostatic voltage plateaus. The oxidation state of Fe would be more precisely understood by X-ray absorption near-edge structure (XANES) analysis; hence, *ex situ* XANES was conducted to investigate the redox behavior during electrochemical reaction in aqueous electrolytes, as shown in Fig. 3a. The XANES spectrum is clearly observed to shift to the right during the charging to 0.7 V *vs.* SCE (the green dot in Fig. 2c), indicating the oxidation of iron towards Fe^{3+}. FeO and Fe_2O_3 were used as the Fe^{2+} and Fe^{3+} references, respectively. The XANES spectrum is also confirmed to shift back to lower valence states after the discharging process. The oxidation state of Fe at −0.2 V *vs.* SCE (the blue dot in Fig. 2c) is placed between Fe^{2+} and Fe^{3+}, which is consistent with the galvanostatic results. To further confirm the change of the electrode after several cycles in aqueous electrolytes, an *ex situ* XRD pattern of the

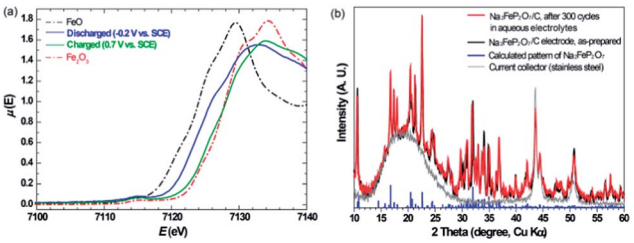

Fig. 3 (a) Fe K-edge XANES spectra of $Na_2FeP_2O_7$/C after charge and discharge between 0.7 and −0.2 V *vs.* SCE in aqueous electrolytes and (b) *ex situ* XRD pattern of $Na_2FeP_2O_7$/C after 300 cycles in aqueous electrolytes.

$Na_2FeP_2O_7$/C electrode after 300 cycles in aqueous electrolytes was collected, as displayed in Fig. 3b. The XRD pattern of the 300-cycled electrode of $Na_2FeP_2O_7$/C does not reveal any degradation or peak changes compared with the fresh electrode. The TEM image and EDS mappings of the cycled $Na_2FeP_2O_7$/C also show no differences to compare with the fresh sample (Fig. S5†).

In summary, this report is the first to examine $Na_2FeP_2O_7$ as a promising electrode material for low cost aqueous SIBs. The $Na_2FeP_2O_7$/C composite enables reversible sodium ion de/insertion into its structure and also demonstrates a high rate capability, robust capacity retention and high stability in an aqueous environment. The remaining challenging point is the relatively low operating voltage of $Na_2FeP_2O_7$; hence, a further study will be focused on enhancing the potential by modulating the redox couples of other transition metal elements or doping with an anion species.

Acknowledgements

This work was supported by the Program to Solve Climate Changes (NRF-2010-C1AAA001-2010-0029031) and Basic Science Research Program (2009-0094038) through the National Research Foundation of Korea (NRF) funded by the Ministry of Science, ICT & Future Planning. The authors thank the Pohang Accelerator Laboratory, Korea for extending the synchrotron XRD and XAFS beamline for characterization.

Notes and references

1 M. D. Slater, D. Kim, E. Lee and C. S. Johnson, *Adv. Funct. Mater.*, 2013, **23**, 947.
2 H. L. Pan, Y. S. Hu and L. Q. Chen, *Energy Environ. Sci.*, 2013, **6**, 2338.
3 V. Palomares, M. Casas-Cabanas, E. Castillo-Martinez, M. H. Han and T. Rojo, *Energy Environ. Sci.*, 2013, **6**, 2312.
4 W. Li, J. R. Dahn and D. S. Wainwright, *Science*, 1994, **264**, 1115.
5 Y. Wang, J. Yi and Y. Xia, *Adv. Energy Mater.*, 2012, **2**, 830.
6 J. F. Whitacre, A. Tevar and S. Sharma, *Electrochem. Commun.*, 2010, **12**, 463.
7 A. D. Tevar and J. F. Whitacre, *J. Electrochem. Soc.*, 2010, **157**, A870.

8 C. D. Wessells, R. A. Huggins and Y. Cui, *Nat. Commun.*, 2011, **2**, 550.
9 C. D. Wessells, S. V. Peddada, R. A. Huggins and Y. Cui, *Nano Lett.*, 2011, **11**, 5421.
10 J. F. Whitacre, T. Wiley, S. Shanbhag, Y. Wenzhuo, A. Mohamed, S. E. Chun, E. Weber, D. Blackwood, E. Lynch-Bell, J. Gulakowski, C. Smith and D. Humphreys, *J. Power Sources*, 2012, **213**, 255.
11 S. I. Park, I. Gocheva, S. Okada and J.-i. Yamaki, *J. Electrochem. Soc.*, 2011, **158**, A1067.
12 Z. Li, D. Young, K. Xiang, W. C. Carter and Y. M. Chiang, *Adv. Energy Mater.*, 2013, **3**, 290.
13 X. Y. Wu, Y. L. Cao, X. P. Ai, J. F. Qian and H. X. Yang, *Electrochem. Commun.*, 2013, **31**, 145.
14 H. Kim, R. A. Shakoor, C. Park, S. Y. Lim, J. S. Kim, Y. N. Jo, W. Cho, K. Miyasaka, R. Kahraman, Y. Jung and J. W. Choi, *Adv. Funct. Mater.*, 2013, **23**, 1147.
15 T. Honma, T. Togashi, N. Ito and T. Komatsu, *J. Ceram. Soc. Japan*, 2012, **120**, 344.
16 P. Barpanda, T. Ye, S. Nishimura, S. C. Chung, Y. Yamada, M. Okubo, H. S. Zhou and A. Yamada, *Electrochem. Commun.*, 2012, **24**, 116.
17 K. H. Ha, S. H. Woo, D. Mok, N. S. Choi, Y. Park, S. M. Oh, Y. Kim, J. Kim, J. Lee, L. F. Nazar and K. T. Lee, *Adv. Energy Mater.*, 2013, **3**, 770.
18 C. S. Park, H. Kim, R. A. Shakoor, E. Yang, S. Y. Lim, R. Kahraman, Y. Jung and J. W. Choi, *J. Am. Chem. Soc.*, 2013, **135**, 2787.
19 P. Barpanda, J. C. Lu, T. Ye, M. Kajiyama, S. C. Chung, N. Yabuuchi, S. Komaba and A. Yamada, *RSC Adv.*, 2013, **3**, 3857.
20 P. Barpanda, T. Ye, M. Avdeev, S. C. Chung and A. Yamada, *J. Mater. Chem.A*, 2013, **1**, 4194.
21 P. Barpanda, G. Liu, C. D. Ling, M. Tamaru, M. Avdeev, S. Chung, Y. Yamada and A. Yamada, *Chem. Mater.*, 2013, **25**, 3480.
22 F. Erragh, A. Boukhari, F. Abraham and B. Elouadi, *J. Solid State Chem.*, 2000, **152**, 323.
23 D. J. Kim, R. Ponraj, A. G. Kannan, H. W. Lee, R. Fathi, R. Ruffo, C. M. Mari and D. K. Kim, *J. Power Sources*, 2013, **244**, 758.

